Grain size and flow volume effects on granular flow mobility in numerical simulations: 3-D discrete element modeling of flows of angular rock fragments

B. Cagnoli[1], and A. Piersanti[1]

[1]Istituto Nazionale di Geofisica e Vulcanologia, Via di Vigna Murata 605, 00143 Rome, Italy.

Correspondence to:

B. Cagnoli

bruno.cagnoli@ingv.it

Key Points:

Discrete element modeling predicts the relative mobility of granular flows

The finer the grain size, the larger the mobility of the centre of mass

The larger the flow volume, the smaller the mobility of the centre of mass

This article has been accepted for publication and undergone full peer review but has not been through the copyediting, typesetting, pagination and proofreading process which may lead to differences between this version and the Version of Record. Please cite this article as doi: 10.1002/2014JB011729

Abstract The results of three-dimensional discrete element modeling (DEM) presented in this paper confirm the grain size and flow volume effects on granular flow mobility that were observed in laboratory experiments where batches of granular material traveled down a curved chute. Our numerical simulations are able to predict the correct relative mobility of the granular flows because they take into account particle interactions and, thus, the energy dissipated by the flows. The results illustrated here are obtained without prior fine tuning of the parameter values to get the desired output. The grain size and flow volume effects can be expressed by a linear relationship between scaling parameters where the finer the grain size or the smaller the flow volume, the more mobile the centre of mass of the granular flows. The numerical simulations reveal also the effect of the initial compaction of the granular masses before release. The larger the initial compaction, the more mobile the centre of mass of the granular flows. Both grain size effect and compaction effect are explained by different particle agitations per unit of flow mass that cause different energy dissipations per unit of travel distance. The volume effect is explained by the backward accretion of the deposits that occurs wherever there is a change of slope (either gradual or abrupt). Our results are relevant for the understanding of the travel and deposition mechanisms of geophysical flows such as rock avalanches and pyroclastic flows.

Keywords:

Discrete Element Modeling; Flows of Rock Fragments; Grain Size; Flow Volume; Mobility

1. Introduction

In this paper, we illustrate 3-D discrete element modeling (DEM) of dry and dense granular flows of angular rock fragments that travel down a curved chute. The purpose of this work is to investigate the reproducibility by numerical simulations of the effects of grain size and flow volume on flow mobility that were observed in laboratory experiments by *Cagnoli and Romano* [2012a]. Both laboratory experiments and numerical simulations are meant to understand the travel and deposition mechanisms of dry and dense geophysical flows. Examples of these flows in nature include pyroclastic flows (such as block-and-ash flows generated by volcanic dome collapses) and rock avalanches [e.g., *Cas and Wright*, 1988; *Pudasaini and Hutter*, 2006]. Regarding pyroclastic flows, our results concern their dense underflows which travel underneath overriding turbulent clouds. The assessment of the hazards due to these flows (which can have significantly large momentum contents) requires the prediction of their mobility. However, the presence of water [e.g., *Legros*, 2002] cannot affect this mobility in pyroclastic flows and rock avalanches that are dry. It is for this reason that, to understand the energy dissipation mechanisms of the flows, we focus here on the interactions of the solid particles.

The prediction of the mobility of geophysical flows is one of the main research goals in the earth sciences. This prediction is however hindered by the approximations adopted by many computer models which bypass the granular nature of the flows and overshadow the complexity of particle interactions. These interactions affect energy dissipation and flow mobility. It is thus no surprise that these models are unable to predict runouts. In depth-averaged models, for example, where flow properties are vertically averaged, these

predictions depend on adjustments by trial and error of input parameters, rheology and stopping criteria. But, by means of fine-tuning many variables, data fitting alone does not prove that nature behaves as the model assumes [*Dyson*, 2004].

Therefore, we adopt here a discrete element modeling because it considers particle-particle and particle-boundary interactions and, thus, it is able to estimate the energy dissipated by the flows. It is because of this feature that discrete element methods provide simulations that we believe to be the most promising as far as the prediction of geophysical flow mobility is concerned. Comparisons between discrete element modeling and laboratory experiments include *Valentino et al.* [2008], *Banton et al.* [2009], *Girolami et al.* [2012], *Yohannes et al.* [2012] and *Mollon et al.* [2012]. The main limitation in the use of discrete element models is that, with today technology, the computational time of the simulations becomes prohibitively large when the actual number of particles found in natural geophysical flows is considered. Our research focuses on fundamental properties of granular flows (such as the effects of grain size and flow volume on flow mobility), which are basic, key features that any model must be able to predict to be considered useful. These effects need to be understood before more complexity is added to the modeling. For example, in gas-fluidised granular flows (but only with grain size finer than 350 μm), high pore pressure generates an upward gas percolation that is hypothesized to be able to reduce the overall basal friction in natural pyroclastic flows [*Sparks*, 1978; *Chedeville and Roche*, 2014]. However, our numerical simulations demonstrate that fine-grain-size flows do not need gas intervention to have higher mobility because there is neither interstitial air nor any other interstitial gas in the model.

The laboratory experiments carried out by *Cagnoli and Romano* [2012a] showed that the finer the grain size of granular flows of angular rock fragments (all the other features the

same), the more mobile their centre of mass. This is due to the smaller energy dissipation per unit of flow mass as grain size decreases. These laboratory experiments showed also that the larger the flow volume (all the other features the same), the smaller the mobility of the centre of mass. This is due to the fact that, on a slope change (either gradual or abrupt), a deposit accretes backward during its formation, and, this accretion is more extended with larger-volume flows because of the larger quantity of granular material that accumulates at the back. In this paper, discrete element modeling confirms the same grain size and flow volume effects on flow mobility that were observed in the laboratory experiments by *Cagnoli and Romano* [2012a]. Importantly, this result is obtained without prior parameter tuning. The generalization provided by the numerical simulations demonstrates the scale invariance of these effects.

Our volume effect does not contradict the conclusions obtained by *Scheidegger* [1973] who reported a different phenomenon. In the paper by *Scheidegger* [1973], his apparent coefficient of friction decreases as flow volume increases because his coefficient is computed taking into account the frontal end of the deposits which becomes more distal as flow volume increases. This is due to the fact that the larger the flow volume, the larger the longitudinal spreading of the deposit [*Davies*, 1982]. We observed the increase of the longitudinal spreading of larger volume deposits in our experiments as well [*Cagnoli and Romano*, 2012a]. It is to avoid the effect of spreading that we estimate our apparent coefficient of friction in both the laboratory experiments and the numerical simulations by considering the displacement of the centre of mass. It is the mobility of the centre of mass that tells us which flow is intrinsically more or less energetically dissipative as a consequence of its own characteristics (such as the size of the rock fragments).

2. Characteristics of the Previous Laboratory Experiments

The results of the laboratory experiments that we generalize in this paper by means of numerical simulations were described by *Cagnoli and Romano* [2012a]. In the laboratory, the experimental apparatus consisted of a straight metallic upper ramp (the accelerator) and a curved chute (Figure 1). The granular material was placed behind a sliding gate located 22.3 cm above x=0 (where this distance is measured along the accelerator). The gate was removed manually to start the experiments. The hyperbolic sine equation of the longitudinal profile of the curved chute,

$$z = 0.3 - 0.085\,\mathrm{arcsinh}(11.765\,x) \tag{1}$$

(where the variables are in meters), is a slightly modified version of the profile of Mayon volcano in the Philippines [*Becker*, 1905]. Both accelerator and chute had the same trapezoidal cross section that corresponds, in nature, to a V-shaped topographic incision with sediment infilling in the centre. The trapezoidal surface of the chute was made of plaster whose roughness was everywhere significantly smaller than the smaller grain size used. The curved chute was 5.4 cm wide and its horizontal length was 1.4 m. This apparatus was used by *Cagnoli and Romano* [2012b] also to measure the granular pressures at the base of the flows by means of a load cell. The pressure profiles showed that particle collisions affect importantly the basal interactions of rapid granular flows that travel on a subsurface with asperities. *McCoy et al.* [2013] recorded similar profiles in the field which confirm the importance of basal collisions in natural flows.

In the laboratory experiments, the mixtures of angular rock fragments had three relatively

narrow grain size ranges: 0.5-1, 1-2 and 2-3 mm. These mixtures were obtained by crushing an aphanitic volcanic rock block (density ~ 2700 kg/m^3) and sieving the fragments. For each grain size range, two different masses (30 g and 60 g) of granular material were used. In these experiments, which were carried out in a controlled environment, only grain size and flow volume changed. The values of all the other variables that can affect flow mobility were constant.

3. Method

3.1. Particles and Apparatuses of the Numerical Simulations

We have generated by means of a CAD software (Rhinoceros 3D) a virtual version (Figure 2) with the same shape and the same size of the apparatus used in the laboratory experiments by *Cagnoli and Romano* [2012a]. The flow movement is triggered by removing the gate behind which the granular mass is at rest before motion. The gate has the same location and it is removed (by sliding it in a direction normal to that of the accelerator) as in the laboratory apparatus. In the laboratory experiments the accelerator had a friction smaller than that of the chute to enable larger travel distances. In the numerical simulations, we use two versions of the same apparatus to assess the effect of the friction of the accelerator: a first version where the accelerator has the same friction coefficient of the chute (0.9) and a second version where the friction coefficient of the accelerator (0.1) is smaller than that of the chute (0.9).

The values of the physical properties of particles and slope in the numerical simulations (Tables 1 and 2) are different from those in the laboratory experiments. These differences are

not a problem here because the flow behaviours we investigate are not restricted to specific values of the physical properties (such as a given value of basal friction). Therefore, our numerical simulations are not meant to reproduce the identical mobility values observed in the laboratory. It is the relative mobility observed in the laboratory that the numerical modeling must show to be considered useful. This relative mobility results in a linear relationship where the centre of mass of the granular flows becomes more mobile as grain size decreases or as flow volume decreases [*Cagnoli and Romano*, 2012a].

Table 1 shows the values of the physical properties of particles, chute and gate used in the numerical simulations. The properties of the particles are those of an igneous rock, the properties of the chute are those of clay and the properties of the gate are those of aluminum. Tables 2 shows the values of the properties that govern particle-particle, particle-chute and particle-gate interactions. These values indicate that we are simulating flows of rock fragments that travel on a subsurface made of soil [*Peng*, 2000]. When the accelerator has not the same properties of the chute (i.e., those of clay), it has those of aluminum. The angle of internal friction of the granular material is not explicitly mentioned by the model, but, this important property is determined by the shapes of the particles. Therefore, the numerical simulations pertain to angular fragments as the laboratory experiments. The surface of the gate in the numerical simulations has a very small friction value to avoid disturbing the granular material when the gate is removed (as in the laboratory experiments).

The numerical flows are dry and consist of particles with three different shapes. We use particles with a cubic shape, half a cubic shape and a quarter of a cubic shape (Figure 3). These polyhedrons represent an equant, an oblate and a prolate particle, respectively. Our flows are, thus, more realistic than flows of particles with only one single shape because

natural geophysical flows contain particles with different shapes. Concerning grain size, we adopt geometrically similar polyhedrons whose longer edges can be 1, 1.5, 2 or 3 mm in length. Only one grain size is used in each granular flow. Three different flow masses are adopted: approximately equal to 9, 13 and 27 g, respectively (particle density is 2700 kg/m^3). These values are similar to those selected in the laboratory experiments, where the range of grain size in each granular mass was deliberately narrow to enable the comparison of the effects of distinctively different grain sizes. The proportion of each particle shape is always the same in all flows irrespective of grain size or flow mass: the equant particles are 38%, the oblate particles 22% and the prolate particles 40% of the flow masses. However, to enable a comparison, ancillary numerical simulations are carried out also with 27 g flows of only cubic particles that are 1 mm in grain size.

The software we use needs to be told where to locate the particles at time zero. For this purpose, we generate, behind the gate, three-dimensional abstract spaces that are filled (before the gate is removed) with particles in random position and without interpenetration. These abstract spaces do not represent any real material object. We use three abstract spaces whose volumes are proportional to the granular masses so that the same compaction and density of the granular material behind the gate before release is obtained. The particles are in contact with one another within these abstract spaces where the average density of the granular masses is 731 ± 23 kg/m^3. Ancillary numerical simulations have been carried out also by filling the larger abstract space with the 9 g and the 13 g granular masses to obtain smaller initial compactions before release. Although the particles of these smaller granular masses within the larger abstract space are in contact with one another, the densities of the granular masses are smaller (248 kg/m^3 in the case of the 9 g masses and 356 kg/m^3 in the case of the 13 g masses) since they are less compacted. In the numerical simulations we use

granular masses that are smaller than those in the laboratory to deal with smaller numbers of particles and, consequently, manageable computing times. The flows with the largest number of particles (~23300) are those with the three particle types, a total mass equal to 27 g and a grain size equal to 1 mm. The flows with the smallest number of particles (~630) are those with the three particle types, a total mass equal to 27 g and a grain size equal to 3 mm.

3.2. Contact Model of the Numerical Simulations

Our 3-D discrete element modeling has been carried out by using the software EDEM developed by DEM Solutions (www.dem-solutions.com). The approach that EDEM adopts when dealing with particles is twofold. On one hand, it adopts the mass, volume and moment of inertia of the polyhedrons we have chosen. On the other hand, it uses clusters of spheres inscribed within the polyhedrons (Figure 3) to estimate impact forces during particle collisions. These forces are a function of sphere overlaps. Clusters of spheres are an effective method to model complex particle shapes with a reasonable degree of approximation. This method allows good computing performance because the contact detection algorithm for clusters of spheres is more efficient than that for polyhedrons. These clusters of spheres (Figure 3) provide a good approximation of angular fragments probably because the clusters and the polyhedrons have a sufficiently similar distribution of the mass in the different directions in space. For particle collisions, the model computes normal and tangential forces, their damping components and the tangential and rolling friction forces [*DEM Solutions*, 2014].

The normal force [*Hertz*, 1882] is

$$F_n = \frac{4}{3} E^* \sqrt{R^*} \lambda_n^{3/2}, \tag{2}$$

where λ_n is the normal overlap, E^* is the equivalent Young's modulus and R^* is the equivalent radius that are defined as follows:

$$\frac{1}{E^*} = \frac{(1-\nu_i^2)}{E_i} + \frac{(1-\nu_j^2)}{E_j} \tag{3}$$

and

$$\frac{1}{R^*} = \frac{1}{R_i} + \frac{1}{R_j}, \tag{4}$$

respectively. Here, E and ν are the Young's moduli and the Poisson's ratios, respectively, of the interacting elements i and j (polyhedrons, chute or gate). R_i and R_j are the radii of the interacting spheres of the interacting polyhedrons i and j. When one of the two interacting elements is not a particle, the equivalent radius is equal to the radius of the interacting sphere of the polyhedron.

The tangential force [*Mindlin,* 1949; *Mindlin and Deresiewicz,* 1953] is

$$F_t = -S_t \lambda_t, \tag{5}$$

where λ_t is the tangential overlap and S_t is the tangential stiffness which is a function of the equivalent shear modulus G^*. The stiffness is

$$S_t = 8G^* \sqrt{R^* \lambda_n} \tag{6}$$

and the equivalent shear modulus is

$$\frac{1}{G^*} = \frac{(2-\nu_i)}{G_i} + \frac{(2-\nu_j)}{G_j}, \tag{7}$$

where G_i and G_j are the shear moduli of the interacting elements. The tangential force is limited by Coulomb's friction which is equal to $\mu_s F_n$, where μ_s is the coefficient of static friction [*Cundall and Strack*, 1979].

The normal and tangential damping components [*Tsuji et al.*, 1992] are

$$F_n^d = -2\sqrt{\frac{5}{6}}\,\varepsilon \sqrt{S_n m^*}\, u_n^{rel} \tag{8}$$

and

$$F_t^d = -2\sqrt{\frac{5}{6}}\,\varepsilon \sqrt{S_t m^*}\, u_t^{rel}, \tag{9}$$

respectively. In equations (8) and (9),

$$\varepsilon = \frac{\ln e}{\sqrt{\ln^2 e + \pi^2}}, \tag{10}$$

$$m^* = \left(\frac{1}{m_i} + \frac{1}{m_j} \right)^{-1} \tag{11}$$

and

$$S_n = 2\, E^* \sqrt{R^*\, \lambda_n}\,, \tag{12}$$

where m^* is the equivalent mass, m_i and m_j are the masses of the interacting elements (polyhedrons, chute or gate), e is the coefficient of restitution, S_n is the normal stiffness and the u^{rel} values are the normal (subscript n) and tangential (subscript t) components of the relative velocity.

The rolling friction [*Sakaguchi et al.*, 1993] is accounted for by applying a torque

$$\tau_i = -\mu_r\, F_n\, d_i\, \omega_i \tag{13}$$

to the contacting surfaces. Here μ_r is the coefficient of rolling friction, d_i is the distance from the centre of mass of the polyhedron to the contact point (where the contact point is defined in the middle of the overlap) and ω_i is the unit angular velocity vector of the particle at the contact point. This torque is calculated independently for each polyhedron.

3.3. Scaling Parameters in the Laboratory Experiments and Numerical Simulations

In both the laboratory experiments [*Cagnoli and Romano*, 2012a, 2012b] and the numerical simulations, the deposited granular material consists of two portions: a more proximal heap that is much more elongated than thick (the deposit of the flow proper) and a more distal distribution of individual fragments. The distal distribution is formed by fragments, which, bouncing within the chute, traveled individually without interacting and are not part of the flow proper. Flows and distal distributions have different movement and depositional mechanisms and they must be considered separately. Here we study only the flow proper.

The reciprocal of mobility is measured, in both the laboratory experiments and the numerical simulations, by computing the ratio of the vertical drop h of the centre of mass of the granular mass to its horizontal displacement l:

$$\mu_A = \frac{h}{l}. \tag{14}$$

A value of μ_A is computed for the final deposit of the flow proper which consists of all the particles on the chute that touch one another. The particles of the distal distribution are those that do not touch one another. We add to each μ_A value of the flow proper an uncertainty bar whose extremities are computed as follows. The upper extremity is the h/l value of the portion of deposit whose distal end is 3 cm in a more proximal position than the distal end of our best estimate of the deposit of the flow proper. The lower extremity is the h/l value of all the particles on the chute (deposit of the flow proper plus distal distribution). Even if there is some uncertainty when locating the position of the distal end of the deposit of the flow

proper, it is clear that the 3 cm shorter deposit and all the particles on the chute provide *h*/*l* values that can be significantly different from the true μ_A value of the flow proper. In particular, the likelihood that the true μ_A value of the flow proper is located somewhere along the uncertainty bar decreases quickly to zero at a relatively short distance from our best estimate.

In the numerical simulations, the *h/l* values are always estimated by discarding the particles of the distal distribution from the final deposits. A set of *h/l* values is however computed also by discarding the particles of the distal distribution from both the final deposits and the granular masses behind the gate before release. The discarding of these particles from behind the gate is a data processing that is impossible in the laboratory experiments where it is impossible, when calculating *h/l*, to identify and remove the particles that will form the distal distribution at the end of the experiment from the granular mass behind the gate before release. In the numerical simulations, the *h/l* values are always computed taking into account the actual mass and the actual position in space of each particle. This is also impossible to do in the laboratory, where the assumption that the granular masses at rest (both those behind the gate and those of the final deposits) have a uniform density had to be made.

In the laboratory experiments, a linear relationship

$$\mu_A = a\beta + b \tag{15}$$

was obtained between μ_A and parameter

$$\beta = \frac{\delta V^{1/3}}{w^2}, \tag{16}$$

where δ is the grain size, V is the flow volume and w is the channel width [*Cagnoli and Romano*, 2012a]. This equation shows that the finer the grain size or the smaller the flow volume (all the other features the same), the larger the mobility of the centre of mass. This linear relationship between mobility, grain size and flow volume is scale invariant (see the dimensional analysis in *Cagnoli and Romano* [2012a]), so that we expect that any value of grain size and flow volume can enter it. Equation (15) refers to dense flows (i.e., not to turbulent flows) without spurious effects such as those due to electrostatic charges. The density of the flows can span a relatively large range of values as shown by figure 3 in *Cagnoli and Romano* [2012b]. Coefficients *a* and *b* depend on the characteristics of the flow and on those of the slope. Although the distance *w* between channel sidewalls does not change in both the laboratory experiments and the numerical simulations, this distance is expected to affect the mobility of the centre of mass. This is so because the wider the channel, the more room the granular material has to widen laterally so that the rear tail of the deposit is able to become longitudinally shorter. Width *w* can be removed from the parameter when the flows travel down a slope without sidewalls (i.e., in a laterally unconfined flow) and it can be replaced by a different normalisation quantity. We adopt parameter β to characterize the flows in the numerical simulations as well. Here quantity *V* is obtained by summing the individual volumes of all the particles that form the deposit of the flow proper.

3.4. Particle Agitation and Energy Dissipation

We calculate the variance of particle speeds in the transversal direction to compare the

agitation of the particles in the different granular flows. This has been done in the central portions (5 cm long) of all flows to avoid the particles of the distal distributions. The variances are computed every 0.1 seconds from when the particles are behind the gate before release (where the variances are zero) until the final deposition at the end of the experiments (where the variances become zero again). In a downslope-moving granular flow with no particle agitation, the components of particle speeds in the transversal direction (i.e., at 90° to the downslope direction) and their variance are zero. Conversely, with particle agitation, the particles acquire a velocity component in the transversal direction, and, the larger the agitation, the larger the variance of this velocity component. Velocity components in the transversal direction are informative in terms of energy dissipation because they imply energy diverted from the flow direction. Particle agitation in granular flows is due to interactions with the asperities of the containing surfaces (both the lateral and the basal ones) and it consists of the acquisition by the particles of speed components in directions different from the downslope one. We measured the variance of particle transversal speeds also in the granular flows of the laboratory experiments [*Cagnoli and Romano*, 2010; 2012b]. Average squared deviations are used in the definition of the so-called granular temperature as well [*Ogawa*, 1978].

We compute also the energy dissipated per unit of flow mass by the same central flow portions whose variance has been determined (but we have verified that longer portions generate the same results). This energy is that dissipated by the flow particles to reach each position along the chute. The dissipated energy is the difference between the initial (before release, where it is only potential) total energy of all the particles and the total energy that they have in each position along the chute. The total energies are the sum of the translational kinetic energy, the rotational kinetic energy and the potential energy. The energy dissipation data and the variances are compared to explain the effect of particle agitation on flow

mobility.

4. Results

The numerical simulations are three-dimensional so that the flows can be examined in cross-section (Figures 4, 5 and 6) or from the top (Figure 7). As soon as the gate is removed, the flows accelerate down the slope, reach a maximum speed and then decelerate and stop (Figure 4). The deposit accretes backward (as in the laboratory experiments) because the frontal portion of the flow stops before the rear portion which accumulates at the back (Figures 5 and 7). Particles that are not part of the flow proper because they travel individually and form, when at rest, the distal distribution are clearly discernible in front of the flow proper in the images of the numerical simulations (for example at 0.7 sec in Figure 4 and at 0.65 sec in Figure 7). Figure 6 shows that the slope-parallel component of particle velocity decreases downward toward the subsurface as expected in flows that travel in contact with a boundary surface [*Hui and Haff*, 1986; *Iverson*, 1997; *Cagnoli and Manga*, 2004].

Figure 8 illustrates the μ_A versus β data of the granular flows in the numerical simulations where the surfaces of accelerator and chute have the same friction coefficient. In Figure 8, the particles of the distal distribution are discarded when calculating the position of the centre of mass of the final deposits. This figure shows that the flows of three particle types with different grain sizes (1, 1.5, 2 and 3 mm) and different flow masses (27, 13 and 9 g) plot along a straight line when they have the same initial compaction behind the gate before release (the solid diamond, solid circle and solid squares in Figure 8). The numerical simulations, thus, generate a linear relationship between μ_A and β as the laboratory

experiments by *Cagnoli and Romano* [2012a]. The flows whose granular masses have a smaller initial compaction behind the gate before release (open diamond and open circle in Figure 8) do not plot along this same straight line. Also the flow of only cubic particles (open square) does not plot along this same straight line. This figure demonstrates that the mobility of the flows does not depend only on the subsurface asperities (which do not change in our simulations), but it depends also on the features of the flow.

The μ_A values obtained in our simulations are relatively large because they measure the mobility of the centre of mass and not the mobility of the distal end of the flows. The mobility of the distal end is larger than that of the centre of mass because of the longitudinal spreading of the granular mass which increases significantly as the flow volume becomes particularly large [*Scheidegger*, 1973; *Davies*, 1982; *Cagnoli and Romano*, 2012a]. Our simulations refer also to flows (such as rock avalanches and block-and-ash flows) that are not liquefied or gas-fluidised. Furthermore, we have adopted a relatively large value of the coefficient of friction between clasts and chute as initial input (Table 2).

It is worth noting that the uncertainty bars of the 27 g flows of 1 and 2 mm particles (the first and the third solid squares from the left in Figure 8) do not overlap, demonstrating that their μ_A values are significantly different and confirming that μ_A decreases as grain size decreases. The 27 g flow of 3 mm particles (the rightmost solid square in Figure 8) has a very large uncertainty bar. This is due to the fact that the 27 g flow of 3 mm particles has a particularly small number (~630) of relatively large particles so that small errors in the location of the boundary of the deposit of the flow proper generates large errors in the location of the centre of mass. Also the 9 g flow (the solid diamond in Figure 8) has a relatively large uncertainty bar because it is made of a relatively small number of particles.

The most accurate estimate of the linear relationship of μ_A versus β is obtained with flows of large number of particles where the error in selecting the deposit of the flow proper generates a small error in the position of its centre of mass as confirmed by their shorter uncertainty bars. It is worth noting that with the larger number of particles, also the μ_A values of the lower extremities of the uncertainty bars (i.e., the μ_A values computed for all particles on the chute) increase as β increases (Figures 8 and 10) confirming the validity of the trend. The figure suggests that there is an increase of the length of the uncertainty bar towards the right side of the plot. However, it is possible to reduce the length of the uncertainty bar also on the right side of the plot when dealing with larger particles by increasing the mass of the flows.

Figure 8 shows also that, when their granular masses have a smaller initial compaction behind the gate before release, the 9 and 13 g flows of the three 1 mm particle types have μ_A values larger than those of the flows with the larger initial compaction and all the other features the same. In particular, the smaller the initial compaction (i.e., the smaller the granular mass within the same larger abstract space behind the gate), the smaller the mobility of the centre of mass as indicated by the open diamond (9 g mass) that has a μ_A value larger than that of the open circle (13 g mass). Figure 8 shows also that the 27 g flow of only 1 mm cubic particles (open square) has a μ_A value that is larger than that of the 27 g flow of the three 1 mm particle types (solid square).

Figure 9 shows a further processing of the data points that are fitted by a straight line in Figure 8. Here, when calculating the position of the centre of mass (and thus μ_A), we discard the particles of the distal distributions not only from the final deposits (as done in Figure 8), but also from the granular masses behind the gate before motion. This further data processing does not prevent a linear relationship between μ_A and β from occurring as shown by Figure 9.

In Figure 9, we have also discarded, when computing μ_A, a few particles more proximal than the proximal end of the deposit because they appear to have travelled individually without interacting and, thus, they do not belong to the deposit of the flow proper. This proximal tail of particles is here too small to affect significantly the final results. However, the proximal tail could be responsible for an overestimate of μ_A, in particular in flows with a relatively small number of particles (such as the 9 g flows).

Figure 10 illustrates the μ_A versus β data of the granular flows in the numerical simulations where the surface of the accelerator has a friction coefficient smaller than that of the chute. Figure 10 shows that the presence of an accelerator with a smaller friction does not alter the type of functional relationship between μ_A and β (which is always a linear one) for the granular masses with the same initial compaction behind the gate before release. The fact that both Figure 8 and Figure 10 show the same type of functional relationship demonstrates an excellent repeatability of the results of the numerical simulations. Again, both the granular masses of only cubic particles and those with a smaller initial compaction before release do not plot along the same straight line but they have larger μ_A values for the same β values.

Figure 11 illustrates the variances of particle speeds in the transversal direction of the 27 g flows of three particle types and the 27 g flow of only cubic particles whose μ_A and β values are shown in Figure 8. Figure 11 demonstrates that the coarser the grain size of the flow (all the other features the same), the larger the variance during the entire travel time. This figure shows also that the variance of the 27 g flow of only 1 mm cubic particles is larger than that of the 27 g flow of 1 mm three particle types during almost their entire travel time. Figure 12 illustrates the variance in the transversal direction of the flows with 9 g and 13 g masses with larger and smaller initial compactions whose μ_A and β values are shown in Figure 8. At the

beginning, the variances of the flows with smaller initial compaction are significantly larger than those of the flows with larger initial compaction, whereas they become slightly smaller at later times.

The energy calculations demonstrate that the flows with coarser particles are more dissipative per unit of flow mass than the flows with finer particles and all the other features the same (as an example, Figure 13 compares the 1 mm grain size flow and the 2 mm grain size flow). The energy calculations prove also that the flows with lower initial compaction are more dissipative per unit of flow mass than those with larger initial compaction and all the other features the same (example in Figure 14) and that the flow with only cubic particles is more dissipative per unit of flow mass than the flow of three particles types and all the other features the same (Figure 15). The energy differences in these figures are small because they are values per unit of mass, but they are significant, as demonstrated by the fact that they confirm the same relative mobility shown by the μ_A values.

In all final deposits of all flows of particles with three shapes, the cubic particles (i.e., those with larger volume) are larger in number at the top and at the front of the deposits (Figure 16). These segregations that affect the clasts with larger volume are phenomena that are well known to take place in geophysical flows during their motion [*Johnson et al.*, 2012; *Cagnoli and Romano*, 2013]. Both segregations toward the top and toward the front can occur without density contrast between segregating clast and matrix. The segregation toward the top is due to the fact that particle agitation increases downward within the granular flows, with the result that there is always a force which acts on the segregating clast and that points upward so that this clast rises if its weight allows it [*Cagnoli and Romano*, 2013]. The segregation toward the front is due to the fact that the speed of the particles is larger at the top

than at the base of the flow, so that the particles which reach the top move faster toward the front where they accumulate. Since this segregation occurs in all our granular flows where the proportions of particle shapes are always the same (irrespective of grain size, flow volume and initial compaction), it cannot be considered the cause of the effects on flow mobility of grain size, flow volume and initial compaction.

5. Discussion

5.1. Grain Size Effect on Flow Mobility

The numerical simulations (irrespective of the friction value of the accelerator) generate the same grain size effect on flow mobility that was observed in the laboratory experiments by *Cagnoli and Romano* [2012a]. This effect consists in the increase of mobility (i.e., decrease of μ_A) as grain size decreases. This is expressed by the linear relationships between μ_A and β (Figures 8, 9 and 10) and it is the result of the decrease of particle agitation as grain size decreases (all the other features the same). This phenomenon is due to the fact that, as grain size decreases, there are more particles in the granular mass and the agitation due to the interaction with the subsurface asperities penetrates less inside the flow. The smaller the agitation of the particles per unit of flow mass, the smaller the energy dissipated per unit of travel distance. For this reason, the number of particles in a flow is a key quantity that has a determinant effect on flow dynamics. In the laboratory experiments, the decrease of particle agitation as grain size decreases was revealed by measuring the velocity fluctuations of the clasts at the top of the flows [*Cagnoli and Romano*, 2010; 2012b] and by measuring the fluctuations of granular pressure at the base of the flows [*Cagnoli and Romano,* 2012b]. The first set of measurements was carried out by using a high-speed video camera and the second

set by using a load cell. Importantly, the numerical simulations demonstrate that this grain size effect is independent from an upward motion of interstitial air or interstitial gas that seeps through the grains and supports part of their weight (such as with gas fluidisation or autofluidisation), because neither air nor any other gas is present among the particles in the computer modeling.

The variance of particle transversal speed in Figure 11 confirms that, also in the numerical simulations, particle agitation decreases as grain size decreases and this is so during the entire travel time. The numerical simulations prove also that the decrease of agitation is accompanied by a decrease of energy dissipation, as shown by Figure 13 where the finer grain size flow dissipates less energy per unit of flow mass than the coarser grain size flow. We have computed also the averages of the absolute values of particles speeds in the transversal direction that show the same identical trends of the variances. This is so because the larger the particle agitation, the larger the kinetic energy spent in the transversal direction. Thus, the less mobile flows are those that divert more energy toward directions which differ from the downslope one.

The linear relationship between μ_A and β documents the change in mobility of the centre of mass as the granular flows go through the internal structural change caused by the change in grain size. In particular, the finer the grain size (all the other features the same), the smaller the agitation of the particles per unit of flow mass and, thus, the thicker the plug, where the plug is the portion of the flow with a much smaller (but not necessarily zero) particle agitation [*Cagnoli and Manga*, 2004; *Cagnoli and Romano*, 2012a; 2012b]. In rapid granular flows, when the plug is present, most particle agitation is located at the base underneath the plug [*Cagnoli and Romano*, 2013]. Thus, the linear relationship shows that rapid granular

flows with a plug have a relatively more mobile centre of mass. It is important to take into account that also small differences of μ_A values can be meaningful. Let's examine, for example, a range of μ_A values from 0.83 to 0.86. Considering that our chute represents a scaled down mountain valley, a vertical drop of 1000 m in nature corresponds to 1209 m of horizontal displacement when μ_A =0.83, whereas it corresponds to 1165 m of horizontal displacement when μ_A =0.86. This is a difference of ~44 m, which is a relatively large distance in hazard assessments since the size of a house is usually smaller.

5.2. Volume Effect on Flow Mobility

A larger mobility of the centre of mass (i.e., smaller μ_A values) as flow volume decreases is observed when the granular masses with different volumes have the same compaction behind the gate before release. This is expressed by the linear relationship between μ_A and β in Figures 8, 9 and 10. This result is true irrespective of the friction value of the surface of the accelerator (Figures 8 and 10). The volume effect in Figures 8, 9 and 10 is the same effect observed in the laboratory experiments by *Cagnoli and Romano* [2012a] where the granular masses behind the gate had the same maximum degree of compaction before release. This behaviour is reported also by *Okura et al.* [2000] whose rock blocks had always the same regular arrangement (i.e., the same initial compaction) before release.

The decrease of mobility of the centre of mass as flow volume increases is the result of the fact that the deposit accretes backward during its formation on a change of slope, and this is more so when the volume of the flow is larger because more granular material accumulates at the back [*Cagnoli and Romano*, 2012a]. In this case, the larger the quantity of granular material that accumulates at the back, the longer the backward shift of the centre of mass. The

backward accretion occurs because the most distal part of the flow reaches the less steep part of the slope and stop before the rear part, preventing the rear part, and the centre of mass, from travelling further downhill as revealed by high-speed video camera images in the laboratory experiments. This occurs wherever deposition takes place on a slope change, either gradual [*Cagnoli and Romano*, 2012a] or abrupt [*Okura et al.*, 2000]. This phenomenon is clearly visible in both the laboratory experiments and the numerical simulations. On a slope change, the rear portions of a flow (on steeper slopes) push downward the frontal portions and the frontal portions (on less steep slopes) hinder the motion of the rear portions, but, when the front stops, the rear is not able to push the front any further. For example, in the laboratory, the application with a finger of an external downslope force at the back of the final deposit deforms its rear end, but it does not move its front. This demonstrates that the front acts as an effective barrier during deposition. This is confirmed also by the fact that when the speeds of the different portions of a laboratory flow are measured in the same spot of the chute, the rear portions have always a smaller speed than the frontal portions in the same place a few instants before. This is so because the frontal portions, already on less steep slopes, prevent the rear portions from travelling faster (figure 9 in *Cagnoli and Romano* [2012a]).

As far as the deposition of a dense flow is concerned, we envisage two possible scenarios. When the flow has no initial thrust, deposition needs a change of slope steepness. In this case, our laboratory experiments and numerical simulations show that the deposit accretes backward. On the other hand, when the flow has an initial thrust, it is able to travel also on a slope which would not otherwise allow its motion so that it can come to a halt also without a change of slope steepness. In this second case, the deposit does not need to accrete backward. Unfortunately, in nature, the deposition of pyroclastic underflows has never been observed

directly because these flows are always hidden by their overriding turbulent clouds.

5.3. Different Initial Compaction before Release and Flow Mobility

Flows whose granular material has a smaller initial compaction behind the gate before release have their centres of mass which are less mobile (i.e., with larger μ_A values) than the flows with a larger initial compaction and all the other characteristics the same (Figures 8 and 10). This effect needs to be taken into consideration by whoever is interested in carrying out mobility studies in the laboratory and in the field. We explain the compaction effect as due to the fact that more compacted granular masses behind the gate stay more compacted (i.e., with smaller agitation per unit of flow mass) also when traveling down the chute and, for this reason, they dissipate less energy per unit of travel distance. The variances of particle transversal speed show that this initial compaction effect on particle agitation is active at the beginning of the downslope journey (Figure 12). The numerical simulations confirm that this larger initial agitation results in an energy dissipation per unit of mass that is larger in the flows of smaller initial compaction than in those of larger initial compaction during the entire travel distance (Figures 14). The effect of the initial compaction was not observed in the laboratory experiments [*Cagnoli and Romano*, 2012a] where all granular masses had the same maximum degree of compaction before release.

Figures 8 and 10 reveal also that the smaller the granular mass within the same abstract space, the smaller the mobility of the centre of mass as shown by the μ_A values of the open diamonds (9 g mass) that are larger than those of the open circles (13 g mass). This can be explained by the fact that the smaller the granular mass within the same abstract space, the smaller the initial compaction and the larger the energy dissipated per unit of travel distance

when moving down the chute. Figure 12 confirms that the agitation of the 9 g flow is larger than that of the 13 g flow as does the measurement of their energy dissipation.

The flows with smaller compaction before release do not plot along the same straight line of the flows with the same larger compaction. This effect occurs in both apparatuses irrespective of the friction value of the accelerator (Figures 8 and 10). Each degree of compaction is expected to generate its own straight line. Also the results obtained by other authors can be explained by different energy dissipations due to different initial compactions. For example, *Manzella and Labiouse* [2013] reported that the runout of a batch of bricks is larger when their distribution before release is regular than when it is random. This is so, because, the compaction of the blocks that are arranged regularly is larger than that of those that are distributed randomly.

5.4. Flows of Only Cubic Particles and their Mobility

The fact that the 27 g flows of only cubic particles (~9400 in number) have a centre of mass that is less mobile than that of the 27 g flow of the three particle types (with a total of ~23300 clasts), all the other features the same (including grain size), can be explained by the different number of fragments. The number of clasts is smaller in the flow of only cubic particles because the non-cubic polyhedrons are portions of the cubic clasts and the total mass of the flows is the same (27 g). Again, the smaller the number of fragments, the larger the particle agitation per unit of flow mass and the larger the energy dissipated per unit of travel distance [*Cagnoli and Romano*, 2012a]. Figure 11 confirms that the agitation (i.e., the variance) of the particles of the 27 g flows of only cubic particles is larger (during almost the entire travel time) than that of the 27 g flows of the three particle types and the same grain

size. That this larger particle agitation results in a larger energy dissipation per unit of mass is proved by the energy measurements (Figure 15). When these energy measurements are carried out separately for the different particle shapes in the same flow, the different particle shapes appear to give a different contribution to the overall energy dissipation per unit of flow mass. In particular, the cubic particles seem to dissipate slightly more energy than the other shapes, and thus, this particle shape is probably increasing further the energy dissipation of the flows of only cubic particles. The flows of only cubic particles (the open squares in Figures 8 and 10) do not plot along the same straight line of the flows of the three particle types because flows with different proportions of particle shapes are expected to plot along different straight lines. These observations are valid for both apparatuses irrespective of the friction value of the accelerator (Figures 8 and 10).

5.5. Basal Friction and Flow Mobility

The numerical simulations where the accelerator has a friction smaller than that of the chute (Figure 10) generate granular flows whose centre of mass is more mobile (i.e., with smaller μ_A values) than the simulations where the accelerator has the same large friction value of the chute (Figure 8). This confirms, as expected, that basal friction affect flow mobility. Flow behaviour appears independent of basal friction only in granular column failures and dam-break experiments with particles because, in these cases, the granular mass collapses upon itself and most particles move on the layer of the first deposited grains [*Lube et al.*, 2011], but, when this does not happen, basal friction is important also in granular collapses [*Balmforth and Kerswell*, 2005]. The importance of the friction coefficients (for both clasts-clast and clast-boundary interactions) is shown by *Girolami et al.* [2012] as well. Also, the fact that the flows (see Figure 4) travel at a constant maximum speed for a while

(such as in the dam-break experiments by *Chedeville and Roche* [2014]) does not indicate a lack of basal friction which is always set to a value different from zero in our simulations. This constant speed is the result of an overstretched inflection between the acceleration and the deceleration of the granular masses (whose initial and final speeds are zero) in a plot of distance versus time.

6. Conclusions

The 3-D discrete element modeling shows the same grain size and flow volume effects on flow mobility that the laboratory experiments [*Cagnoli and Romano*, 2012a] have revealed. Importantly, this has been obtained without prior adjustment of the values of the parameters to generate the desired results. This proves the usefulness of discrete element modeling. Here, we focus on dry and dense granular flows which have pyroclastic flows (for example block-and-ash flows) and rock avalanches as counterparts in nature.

According to both numerical simulations and laboratory experiments, the mobility of the centre of mass increases as grain size decreases (Figures 8, 9 and 10). This is so because the energy dissipated by the granular flows per unit of flow mass decreases as grain size decreases. In this sense, flows with different grain sizes are like cars with different fuel efficiency engines. The numerical simulations reveal also that the initial compaction of the granular mass behind the gate before release has an important effect on flow mobility. This effect is explained, as the grain size effect, by different particle agitations per unit of flow mass that cause different energy dissipations per unit of travel distance. When the granular masses have all the same initial compaction before release, in both the laboratory experiments and the numerical simulations, the larger the flow volume, the smaller the mobility of the

centre of mass (Figures 8, 9 and 10). This is so because a deposit accretes backward during its formation on a change of slope (either gradual or abrupt) and this rearward accretion is more extended when the granular mass is larger. Therefore, an increase of flow volume can counteract the effect on mobility of a decrease of grain size so that it is the product of these quantities that enters parameter β. All the effects on mobility obtained with the apparatus where accelerator and chute have the same friction have been obtained also with the apparatus where accelerator and chute have different frictions (the accelerator is the upper straight portion of the apparatus whereas the chute is its lower curved portion).

The mobility of the granular flows (see, for example, figure 7 in *Cagnoli and Romano* [2010]) that is inversely proportional to the agitation of the fragments per unit of flow mass (where agitation increases as the number of particles decreases) is an explanation consistent with all the flow behaviours we have observed: those generated when the grain size changes, when the initial compaction changes and when the proportion of particle shapes changes. This confirms the pivotal role that particle agitation has in determining flow dynamics. The effect of a change of subsurface steepness in determining the mobility of the flows when their volume varies is, however, important as well, because a change of slope steepness is needed to trigger deposition.

Extensive research is required before prediction of mobility of geophysical flows as a function of all their features is possible. We believe that this research must focus on particle interactions because they are responsible for the energy dissipated by the granular flows. It is for this reason that discrete element methods provide simulations that are the most promising when predicting the mobility of geophysical flows.

Acknowledgments

We thank G. Mollon, S. Charbonnier and an anonymous reviewer for their useful comments. The data upon which the conclusions of this paper are based are available as supporting information and from the corresponding author on request.

References

Banton, J., P. Villard, D. Jongmans, and C. Scavia (2009), Two-dimensional discrete element models of debris avalanches: Parameterization and the reproducibility of experimental results, *J. Geophys. Res.*, *114*, F04013, doi:10.1029/2008JF001161.

Balmforth, N.J., and R.R. Kerswell (2005), Granular collapse in two dimensions, *J. Fluid Mech.*, *538*, 399-428.

Becker, G.F. (1905), A feature of Mayon Volcano, *Proc. Wash. Acad. Sci.*, *7*, 277-282.

Cagnoli, B., and M. Manga (2004), Granular mass flows and Coulomb's friction in shear cell experiments: Implications for geophysical flows, *J. Geophys. Res.*, *109*, F04005, doi:10.1029/2004JF000177.

Cagnoli, B., and G.P. Romano (2010), Effect of grain size on mobility of dry granular flows of angular rock fragments: An experimental determination, *J. Volcanol. Geotherm. Res.*, *193*, 18-24.

Cagnoli, B., and G.P. Romano (2012a), Effects of flow volume and grain size on mobility of dry granular flows of angular rock fragments: A functional relationship of scaling parameters, *J. Geophys. Res.*, *117*, B02207, doi:10.1029/2011JB008926.

Cagnoli, B., and G.P. Romano (2012b), Granular pressure at the base of dry flows of angular rock fragments as a function of grain size and flow volume: A relationship from laboratory

experiments, *J. Geophys. Res.*, *117*, B10202, doi:10.1029/2012JB009374.

Cagnoli, B., and G.P. Romano (2013), Vertical segregations in flows of angular rock fragments: Experimental simulations of the agitation gradient within dense geophysical flows, *J. Volcanol. Geotherm. Res.*, *265*, 52-59.

Cas, R. A. F., and J. V. Wright (1988), *Volcanic Successions*, Unwin Hyman, London.

Chedeville, C., and O. Roche (2014), Autofluidization of pyroclastic flows propagating on rough substrates as shown by laboratory experiments, *J. Geophys. Res. Solid Earth*, *119*, doi:10:1002/2013JB010554.

Cundall, P.A., and O.D. Strack (1979), A discrete numerical model for granular assemblies, *Geotechnique*, *29*, 47-65.

Davies, T. R. (1982), Spreading of rock avalanche debris by mechanical fluidization, *Rock Mech.*, *15*, 9-24.

DEM Solutions (2014), *EDEM 2.6 Theory Reference Guide*, Edinburgh, United Kingdom.

Dyson, F. (2004), A meeting with Enrico Fermi, *Nature*, *427*, 297.

Girolami, L., V. Hergault, G. Vinay, and A. Wachs (2012), A three-dimensional discrete-grain model for the simulation of dam-break rectangular collapses: comparison between numerical results and experiments, *Granular Matter*, *14*, 381-392.

Hertz, H. (1882), Über die Berührung fester elastischer Körper, *J. Reine Angewandte Mathematik*, *92*, 156-171.

Hui, K., P.K. Haff (1986), Kinetic grain flow in a vertical channel, *Int. J. Multiphase Flow*, *12*, 289-298.

Iverson, R.M. (1997), The physics of debris flows, *Rev. Geophys.*, *35*, 245-296.

Johnson, C.G., B.P. Kokelaar, R.M. Iverson, M. Logan, R.G. La Husen and J.M.N.T. Gray (2012), Grain-size segregation and levee formation in geophysical mass flows, *J. Geophys. Res.*, *117*, F01032, doi:10.1029/2011JF002185.

Legros, F. (2002), The mobility of long-runout landslides, *Eng. Geol.*, *63*, 301-331.

Lube, G., H.E. Huppert, R.S.J. Sparks, and A. Freundt (2011), Granular column collapses down rough, inclined channels, *J. Fluid Mech.*, *675*, 347-368.

Manzella, I., and V. Labiouse (2013), Empirical and analytical analyses of laboratory granular flows to investigate rock avalanche propagation, *Landslides*, *10*, 23-36.

Mindlin, R.D. (1949), Compliance of elastic bodies in contact, *J. Appl. Mech.*, *16*, 259-268.

Mindlin, R.D., and H. Deresiewicz (1953), Elastic spheres in contact under varying oblique forces, *J. Appl. Mech.*, *20*, 327-344.

McCoy, S.W., G.E. Tucker, J.W. Kean, and J.A. Coe (2013), Field measurement of basal forces generated by erosive debris flows, *J. Geophys. Res. Earth Surf.*, *118*, 1-14, doi:10.1002/jgrf.20041.

Mollon, G., V. Richefeu, P. Villard, and D. Daudon (2012), Numerical simulation of rock avalanches: Influence of a local dissipative contact model on the collective behavior of granular flows, *J. Geophys. Res.*, *117*, F02036, doi:10.1029/2011JF002202.

Ogawa, S. (1978), Multitemperature theory of granular materials, *Proceedings of the U.S.-Japan Seminar on Continuum-Mechanics and Statistical Approaches to the Mechanics of Granular Materials*, Tokyo, 208-217.

Okura, Y., H. Kitahara, T. Sammori, and A. Kawanami (2000), The effects of rockfall volume on runout distance, *Eng. Geology*, *58*, 109-124.

Peng, B. (2000), Rockfall trajectory analysis: Parameter determination and application, M.S. thesis, Univ. of Canterbury, Christchurch, New Zealand.

Pudasaini, S.P., and K. Hutter (2006), *Avalanche Dynamics*, Springer, Berlin.

Sakaguchi, E., E. Ozaki, and T. Igarashi (1993), Plugging of the flow of granular materials during the discharge from a silo, *Int. J. Mod. Phys.*, B7, 1949-1963.

Scheidegger, A.E. (1973), On the prediction of the reach and velocity of catastrophic

landslides, *Rock Mech.*, *5*, 231-236.

Sparks, R.S.J. (1978), Gas release rates from pyroclastic flows: An assessment of the role of fluidisation in their emplacement, *Bull. Volcanol.*, *41*, 1, 1-9.

Tsuji, Y., T. Tanaka, and T. Ishida (1992), Lagrangian numerical simulation of plug flow of cohesionless particles in a horizontal pipe, *Powder Technology*, *71*, 239-250.

Valentino, R., G. Barla, and L. Montrasio (2008), Experimental analysis and micromechanical modelling of dry granular flow and impacts in laboratory flume tests, *Rock Mech. Rock Engng.*, *41*, 153-177.

Yohannes, B., L. Hsu, W.E. Dietrich, and K.M. Hill (2012), Boundary stresses due to impacts from dry granular flows, *J. Geophys. Res.*, *117*, F02027, doi:10.1029/2011JF002150.

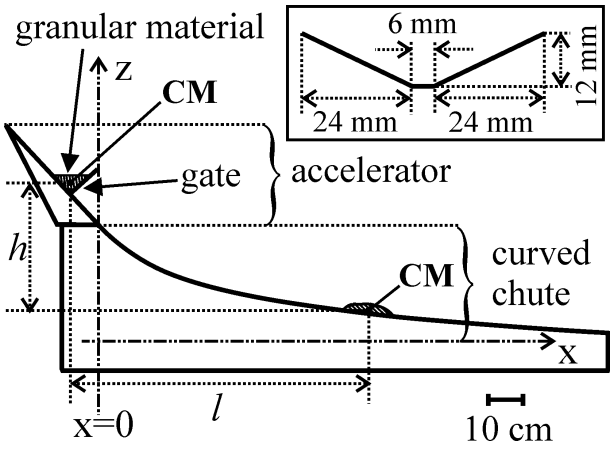

Figure 1. Longitudinal cross-section of the apparatuses used in the numerical simulations and in the laboratory experiments. The inset shows the transversal cross-section of both the accelerator and the chute.

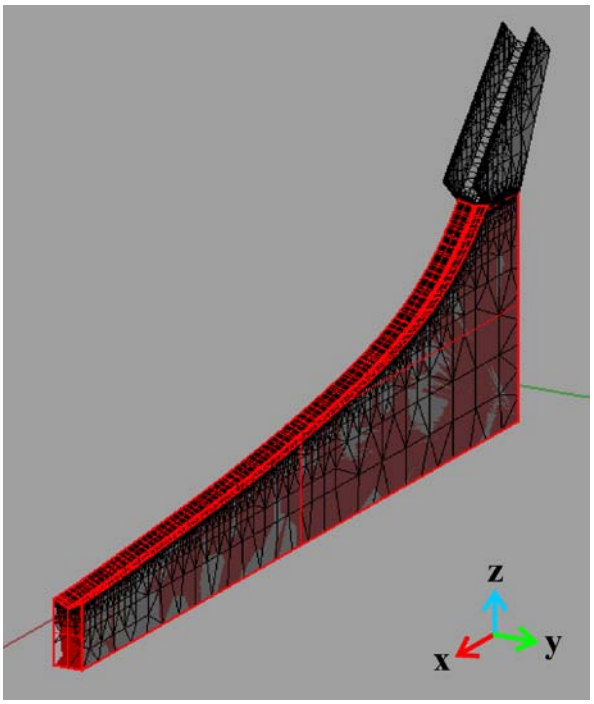

Figure 2. Virtual apparatus generated by means of a CAD software for the numerical simulations.

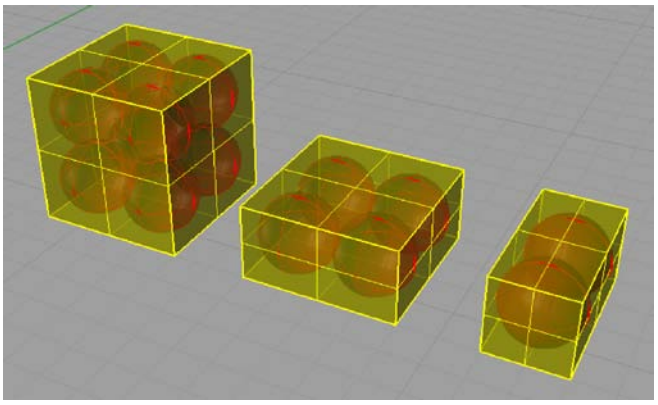

Figure 3. Shapes of the particles (with the inscribed clusters of spheres) that are used in the numerical simulations.

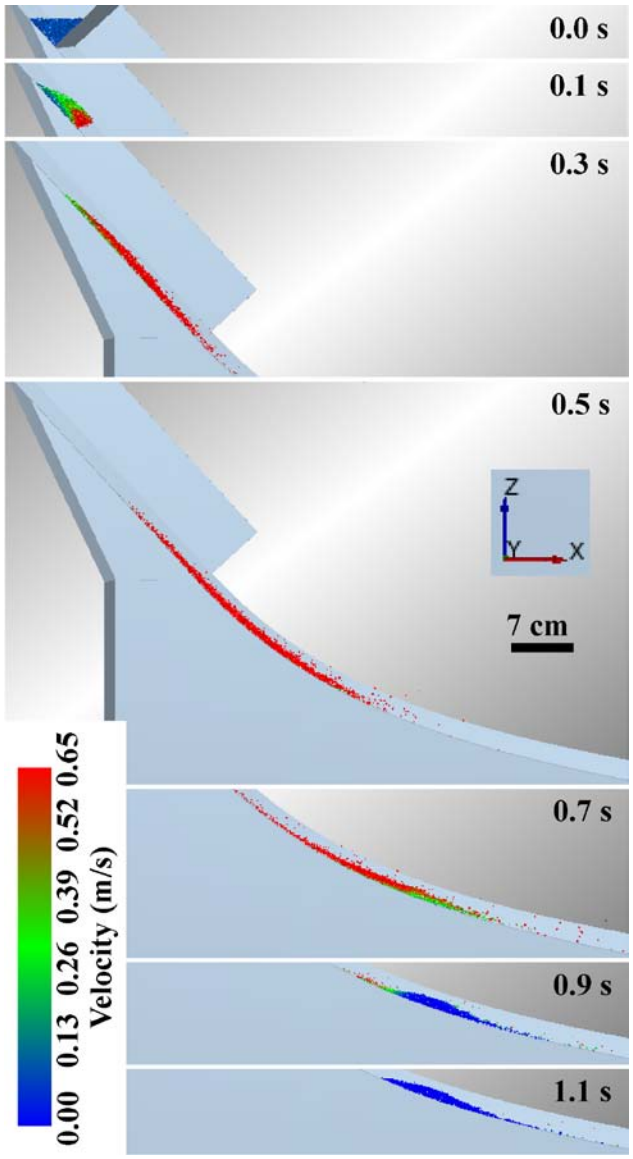

Figure 4. Longitudinal cross-section of a 27 g flow of the three particle types that are 1.5 mm in grain size. In this version of the apparatus, the accelerator and the chute have the same surface friction.

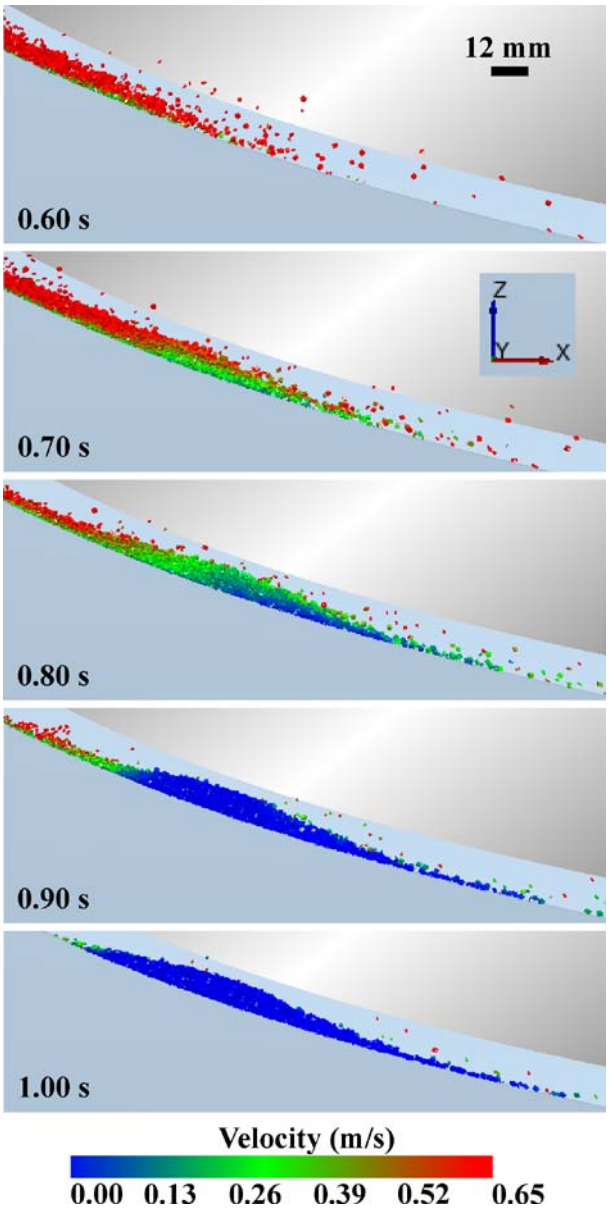

Figure 5. Longitudinal cross-section of the depositing flow of Figure 4.

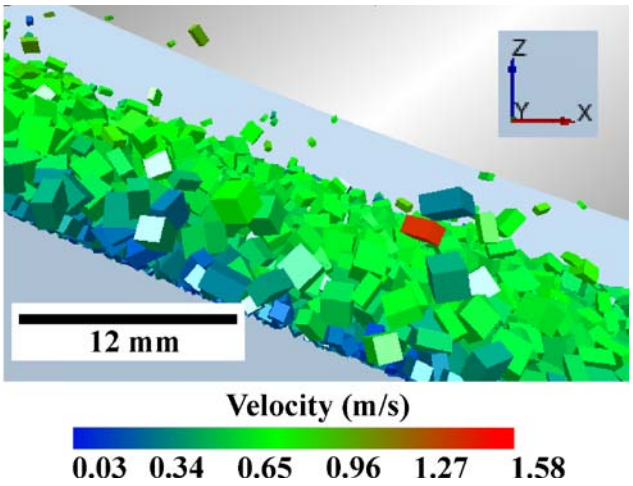

Figure 6. Longitudinal cross-section of a 27 g flow of the three particles types that are 1 mm in grain size. In this version of the apparatus, the accelerator and the chute have the same surface friction. This image shows that the slope-parallel speed of the particles within the flows decreases downward toward the subsurface.

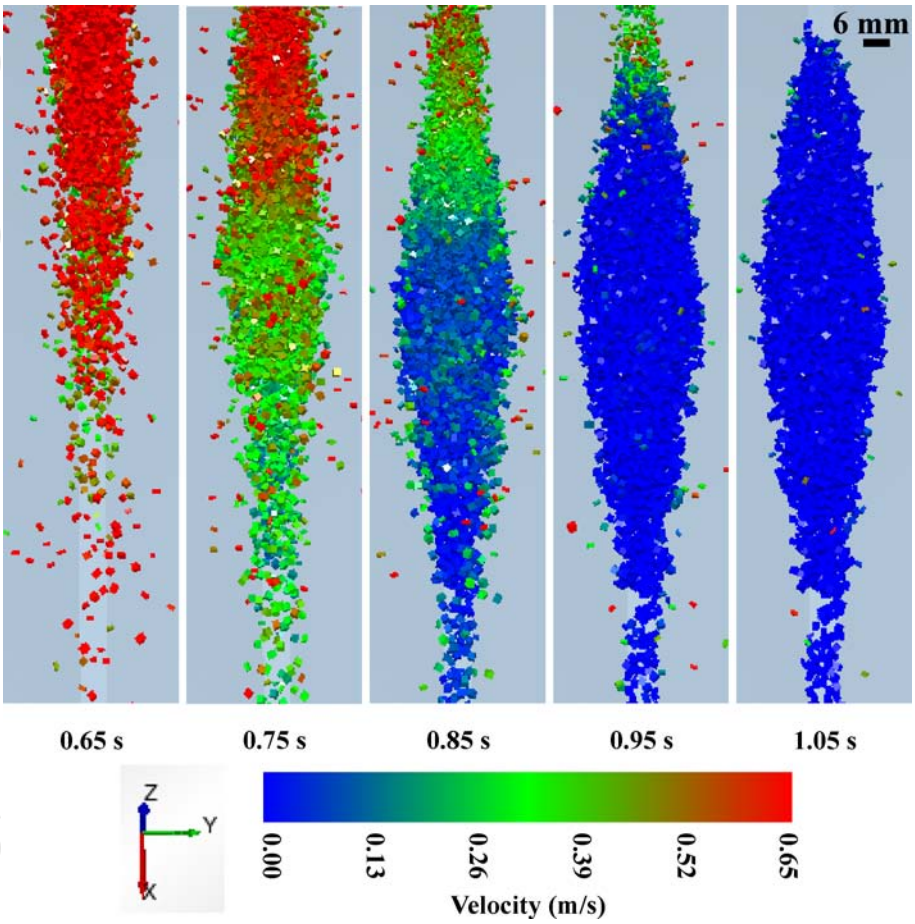

Figure 7. Top view of the depositing flow of Figure 4. The deposit accretes backward.

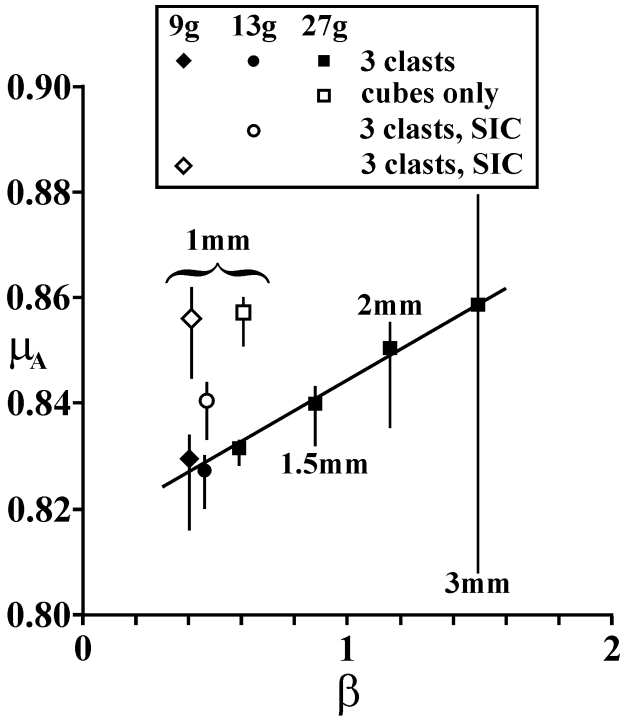

Figure 8. Plot of the μ_A versus β data obtained with the apparatus where accelerator and chute have the same relatively large friction value. SIC stands for smaller initial compaction of the particles behind the gate before motion. The values in millimetres are the grain sizes and those in grams the flow masses. The flows of the three different particle types (3 clasts) and those of only cubic particles (cubes only) are shown with different symbols. The least squares fit to the data is a straight line (here, in equation (15), a = 0.029 and b = 0.8154).

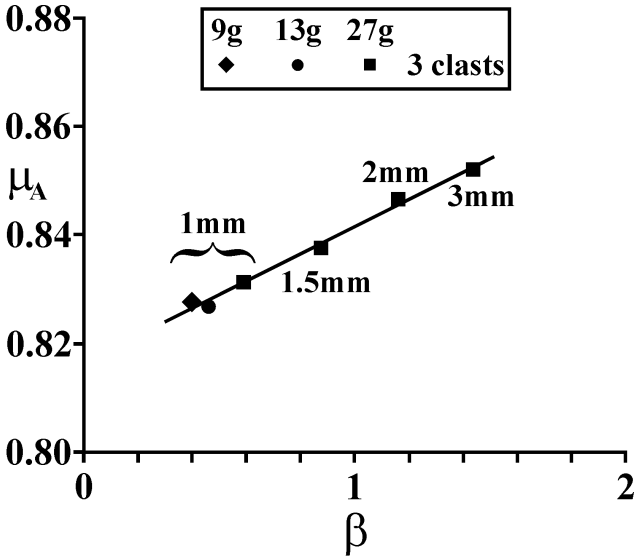

Figure 9. Further processing of the data that plot along the straight line in Figure 8. Here, the values of the parameters are computed discarding the particles of the distal distribution not only from the final deposits (as in Figure 8) but also from the granular masses behind the gate before release. The values in millimetres are the grain sizes and those in grams the flow masses. These are all flows of the three different particle types (3 clasts). The least squares fit to the data is a straight line (here, in equation (15), $a = 0.025$ and $b = 0.8165$).

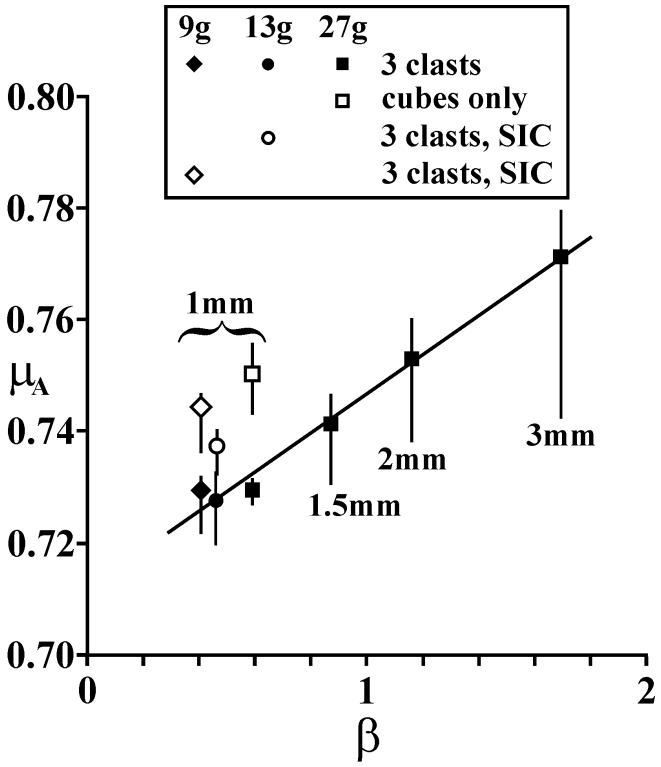

Figure 10. Plot of the μ_A versus β data obtained with the apparatus where the surface of the accelerator has a friction coefficient smaller than that of the chute. SIC stands for smaller initial compaction of the particles behind the gate before motion. The values in millimetres are the grain sizes and those in grams the flow masses. The flows of the three different particle types (3 clasts) and those of only cubic particles (cubes only) are shown with different symbols. The least squares fit to the data is a straight line (here, in equation (15), a = 0.0348 and b = 0.7119).

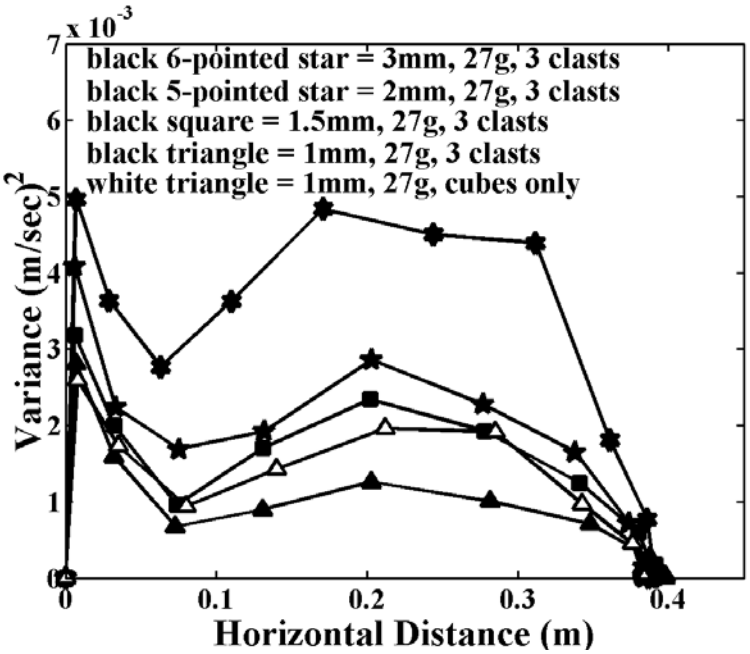

Figure 11. Variances of particle speeds in the transversal direction of the 27 g flows of three particle types (3 clasts) and the 27 g flow of only cubic particles (cubes only) whose μ_A and β values are shown in Figure 8. The values in millimetres are the grain sizes and the values in grams are the flow masses.

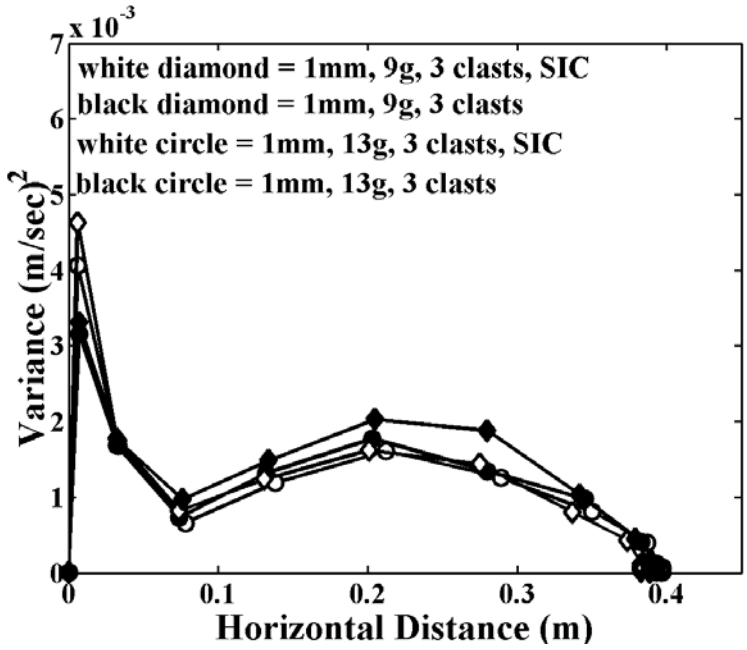

Figure 12. Variances of particle speeds in the transversal direction of the 9 g and 13 g flows of three particle types (3 clasts) with larger and smaller initial compactions before release. The μ_A and β values of these flows are shown in Figure 8. The values in millimetres are the grain sizes and the values in grams are the flow masses. SIC stands for smaller initial compaction of the particles behind the gate before release.

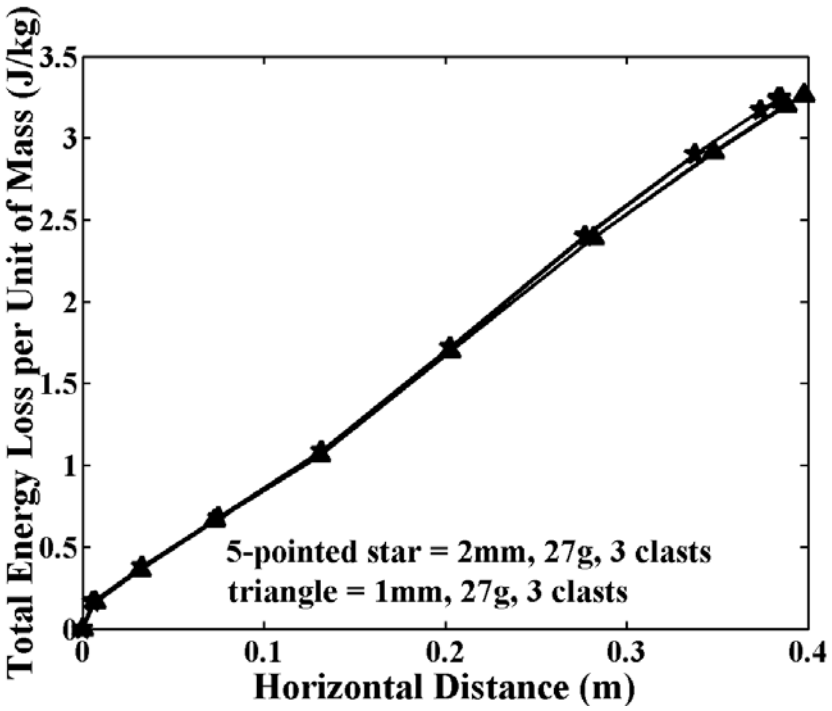

Figure 13. Comparison of the total energy dissipation per unit of flow mass to reach each position along the slope between a coarser (2 mm) and a finer (1 mm) grain size flow (all the other features the same). The μ_A and β values of these flows are shown in Figure 8. These flows of three particle types (3 clasts) have a mass equal to 27 g.

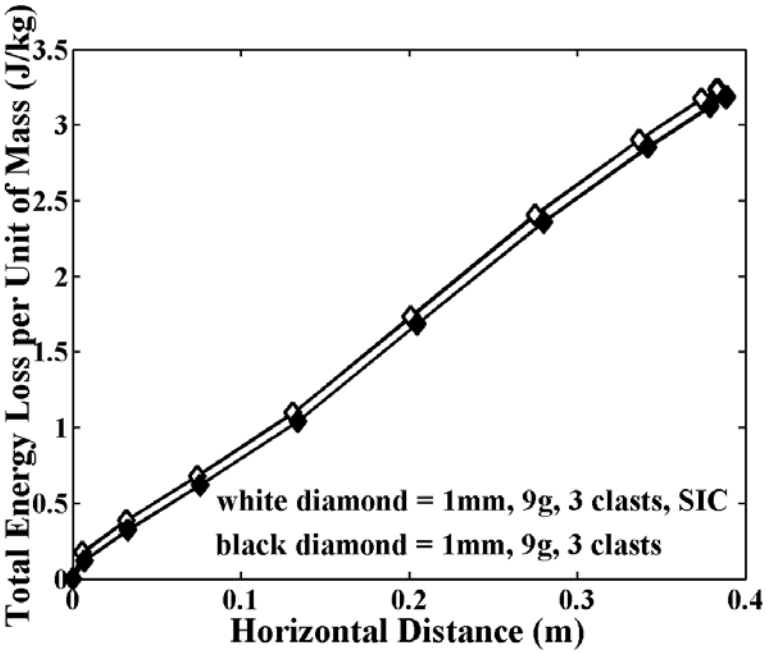

Figure 14. Comparison of the total energy dissipation per unit of flow mass to reach each position along the slope between flows with different initial compactions before release. These flows of three particle types (3 clasts), whose μ_A and β values are shown in Figure 8, have a grain size equal to 1 mm and a mass equal to 9 g. SIC stands for smaller initial compaction of the particles behind the gate before release.

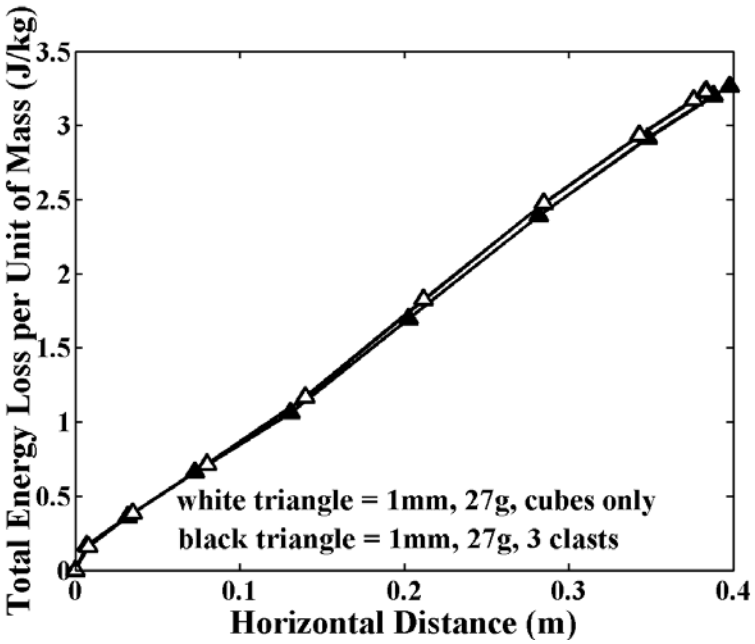

Figure 15. Comparison of the total energy dissipation per unit of flow mass to reach each position along the slope between the flow with only cubic particles (cubes only) and that with three particle types (3 clasts) and all the other features the same. The μ_A and β values of these flows are shown in Figure 8. These flows are 1 mm in grain size and they have a mass equal to 27 g.

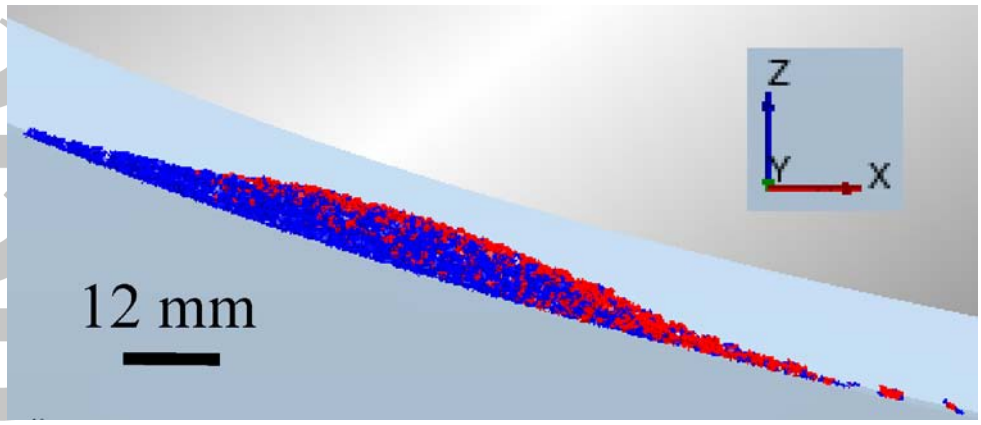

Figure 16. Example of the final deposit in a numerical simulation that shows, in cross-section, that the cubic particles (in red) have segregated toward the top and toward the front during flow motion. This is a deposit of a 27 g flow of three particle types that are 1 mm in grain size.

Table 1. Physical Properties[a] of Materials

	Particles	Chute	Gate
Poisson's Ratio	0.19	0.35	0.36
Shear Modulus (Pa)	2.38e+10	6.85e+09	25e+09
Density (kg/m^3)	2700	2580	2700

[a]When the accelerator has not the same property values of the chute, it has those of the gate.

Table 2. Values of properties[a] governing clast-clast, clast-chute and clast-gate interactions

	Clast-Clast	Clast-Chute	Clast-Gate
Coefficient of Restitution	0.49	0.3	0.53
Coefficient of Static Friction	0.45	0.9	0.1
Coefficient of Rolling Friction	0.035	0.07	0.07

[a]When the accelerator has not the same property values of the chute, it has those of the gate.